X-band EPR imaging as a tool for gradient dose reconstruction in irradiated bones

Philippe Levêque and Quentin Godechal
Biomedical Magnetic Resonance Unit, Université catholique de Louvain, B-1200 Brussels, Belgium

Anne Bol
Molecular Imaging and Experimental Radiotherapy Unit, Université catholique de Louvain, B-1200 Brussels, Belgium

François Trompier
Institut de Sûreté Nucléaire et de Radioprotection, F-92262 Fontenay-aux-Roses, France

Bernard Gallez[a)]
Biomedical Magnetic Resonance Unit, Université catholique de Louvain, B-1200 Brussels, Belgium

(Received 13 March 2009; revised 19 June 2009; accepted for publication 14 July 2009; published 17 August 2009)

Purpose: Various tools are currently available for dose reconstruction in individuals after accidental exposure to ionizing radiation. Among the available biological analyses, Monte Carlo simulations, and biophysical methods, such as electron paramagnetic resonance (EPR), the latter has proved its usefulness for retrospective dosimetry. Although EPR spectroscopy is probably the most sensitive technique, it does not provide spatial dosimetric data. This information is, however, highly desirable when steep dose gradient irradiations are involved. The purpose of this work was to explore the possibilities of EPR imaging (EPRI) for spatial dose reconstruction in irradiated biological material.
Methods: *X*-band EPRI was used to reconstruct *ex vivo* the relative dose distribution in human bone samples and hydroxyapatite phantoms after irradiation with brachytherapy seeds or x rays. Three situations were investigated: Homogeneous, stepwise gradient, and continuous gradient irradiation.
Results: EPRI gave a faithful relative spin density distribution in bone samples and in hydroxyapatite phantoms. Measured dose ratios were in close agreement with the actual delivered dose ratios. EPRI was able to distinguish the dose gradients induced by two different sources (^{125}I and ^{192}Ir). However, the measured spatial resolution of the system was 1.9 mm and this appeared to be a limiting factor. The method could be improved by using new signal postprocessing strategies.
Conclusions: This study demonstrates that EPRI can be used to assess the regional relative dose distribution in irradiated bone samples. The method is currently applicable to *ex vivo* measurements of small size samples with low variation in tissue density but is likely to be adapted for *in vivo* application using *L*-band EPRI. © *2009 American Association of Physicists in Medicine*.
[DOI: 10.1118/1.3194775]

Key words: EPRI, retrospective dosimetry, bones, imaging

I. INTRODUCTION

For years, radioactivity has been used in many different sectors of human activity, including industrial and medical applications. The dangers of ionizing radiation are well known and adequate preventive radioprotection measures are required when using radiation sources.

Although applications involving the use of radioactivity are strictly controlled and generally safe, accidents are always possible and occur each year.[1] These include radiotherapy accidents,[2,3] industrial accidents involving the manipulation of devices used for gammagraphy or radiography containing highly radioactive sources,[4] and handling of lost sources.[5,6]

Different types of irradiation pattern can be observed (whole body exposure vs localized irradiation) and consequences range from no or moderate acute effects to death. As the effects are directly related to the absorbed dose, dosimetry is a key parameter for the optimal medical management of victims. The dose received by individuals may be heterogeneously distributed and should be assessed accurately. Individual dosimeters are useful devices to monitor absorbed dose, but, when accidents occur, victims are usually not wearing a dosimeter at the time of overexposure and irradiation is usually highly heterogeneous. Hence, "after the fact" or retrospective dosimetry is generally required. Although several complementary tools are currently available,[7] actual dose reconstruction remains a difficult task, especially when heterogeneous irradiation with large gradients of dose deposition is suspected.

Models, including numerical simulation (Monte Carlo), have been developed for retrospective dosimetry purposes.[8–11] In this method, the victim and the source must be modeled in terms of geometry and composition; energy deposition in the body is then mathematically calculated.

This methodology has been used for several accidents in the past.[6,12,13] However, for proper modeling, reliable and accurate knowledge of the scenario of the accident is required. This is a major limitation of the method because this kind of information is often lacking or relies on unreliable testimonies.

Biological methods based on cytogenetic assays, such as looking for chromosome aberrations by chromosome painting,[7] can provide valuable dosimetric information but are limited to whole body dosimetry and cannot provide any insight into dose distribution. Moreover, the sensitivity of these techniques is limited.[14]

The biophysical method, which uses electron paramagnetic resonance (EPR) spectrometry, has proved its usefulness in several very serious accidents.[4,15–17] EPR dosimetry studies measure the signal from CO_2^- radicals that are radioinduced in several tissues (bones, teeth enamel).[18–21] The signal intensity is proportional to the dose delivered to the tissue so that calibration is possible and rapid dosimetry is achievable. The intensity-dose relation is linear over a wide range including low doses, and this is probably one of the most sensitive techniques currently available.

A method offering spatial dosimetric information without sampling would be highly desirable, especially when large and steep dose gradient irradiations are involved, for instance when highly active sources are manipulated manually generating a high dose gradient. *X*-band EPR spectroscopy could be used to assess regional dosimetric variations, but that would require multiple invasive tissue samplings.

Possible use of *L*-band EPR spectrometry for noninvasive dosimetry studies of irradiated fingers has also been demonstrated.[22,23] This method offers the advantage of being noninvasive but does not give any spatial information.

EPR imaging (EPRI) combines the information of EPR spectrometry with the possibility of imaging.[24–26] Using a gradient field encoding technique, it is possible to study the spin density distribution within a sample. This method is analogous to MRI, except that the generated image represents the distribution of electron spins instead of nuclear spins. Two modalities can be used. *X*-band EPR works in the high frequency, in the microwave domain (~9 GHz), and offers a very high sensitivity but cannot be used for biological samples because of the increase in the sample temperature due to nonresonant energy absorption by water. A second modality, *L* band, works in a lower frequency domain (~1.2 GHz) and is less sensitive but can be used for humid biological samples, including *in vivo* detection of spins. EPRI combined with *L* band allows to obtain information about spatial distribution of dose in *in vivo* measurements. In a previous work, we have already demonstrated that *L*-band EPRI imaging could be used for dosimetric purposes using lithium formate dosimeter.[27]

In this study, we investigated the possible use of *X*-band EPRI for delineation of spatial spin density distribution in irradiated human bone samples and synthetic hydroxyapatite phantoms. We used *X*-band rather than *L*-band EPR in order to ensure sufficient sensitivity and to prevent nonefficient reconstruction of images that could occur with a low signal-to-noise ratio. Although *X*-band EPRI is limited to *ex vivo* samples, it is an essential step toward development of *in vivo* EPRI using *L* band.

Several irradiation schemes were produced (homogeneous, stepwise gradient irradiation, continuous gradient) using different radioactive sources in order to assess (validate) the possibilities of EPRI in various situations of increasing complexity.

II. MATERIALS AND METHODS

Three types of sample were used: Whole untreated distal phalanxes, bone samples cut from the femur, and phantoms made from hydroxyapatite.

II.A. Bone samples

Distal phalanxes were obtained from the laboratory of anatomy at the Université catholique de Louvain. Samples taken from the dense and compact part of the femur were cut to the desired parallelepiped shape using a small electrical angle grinder machine. The dimensions of the samples were 10.0–15.0 mm (length), 6.0–7.0 (width), and 6.0–6.3 mm (thickness). Absence of any mechanically induced EPR signal was checked before using these samples for the experiments. A hole was drilled in the center of some samples to allow insertion of a radioactive source. The diameter of the hole was 0.8 mm for ^{125}I sources and 0.6 mm for ^{192}Ir sources.

II.B. Hydroxyapatite phantoms

Cylindrical tablets were made from synthetic hydroxyapatite (HAP) (Aldrich, Steinheim, Germany) using a tablet press (Ateliers Courtoy, type AC27, Halle, Belgium, 40 kg/cm^2). The infrared spectrum of the HAP showed a typical band at 872 cm^{-1} which is characteristic of the bone like *B*-type HAP. Paraffin was used as a binding material (15% w/w).[28] Tablets were cut to give the phantoms their final shape (18 mm length $\times$ 6 mm width $\times$ 4.2 mm thickness). A hole was drilled in the center of some samples to allow insertion of a radioactive source. The diameters of the hole were 0.8 mm for ^{125}I sources and 0.6 mm for ^{192}Ir sources.

II.C. Irradiation

The samples were irradiated with different sources of ionizing radiation in order to produce different irradiation schemes: Homogeneous irradiation, stepwise dose gradient, or continuous dose gradient. Homogeneous external irradiation of compact bone and HAP phantoms was performed using either an x-ray beam (Philips 250 RT, 250 kV) with a dose rate of 0.85 Gy min^{-1} or a linear accelerator (Elekta SL 75/5 linac) with a dose rate of 2 Gy min^{-1}. The total dose was 100 Gy. Stepwise gradient irradiation was performed using the same irradiators and appropriate lead shielding. Doses delivered to the different areas were 200, 100, and 0

Gy for the first set of experiment and 300 and 150 Gy in the second one. Continuous gradient irradiation of compact bone and HAP phantoms was carried out using two types of brachytherapy source.

Iodine-125 seeds (Oncoseed model, GE Healthcare) were used to induce a steep dose gradient, as ^{125}I is a low energy gamma emitter (35 keV). The source was either positioned in the center of the sample or stuck on its side. These seeds consist of a welded titanium capsule (0.8 mm diameter, 4.5 mm length) containing ^{125}I adsorbed onto a silver rod (0.5 mm diameter, 3 mm length). Activity was 105 MBq (2.85 mCi) at the beginning of the irradiation period. Iridium-192 wires (LDR, Bebig, Germany, 0.3 mm diameter, 5.0 mm length, activity of 65.5 MBq cm^{-1} or 1.77 mCi cm^{-1}) were selected to produce a smooth dose gradient, ^{192}Ir being a higher energy gamma emitter with a larger range than ^{125}I.

Samples irradiated with the brachytherapy sources were exposed to the source for 3 weeks, protected from light and at room temperature. After irradiation, all samples were kept in the same conditions before being imaged.

Continuous gradient irradiation of the phalanx was performed with a ^{60}Co irradiator (gamma photon emitter, mean energy=1.25 MeV). Samples were placed close to the source (5 cm) and perpendicularly to the isodose to generate a dose gradient along the samples. The maximal dose rate was estimated at 128 Gy min^{-1}. Dosimetry was performed with alanine dosimeters measured by *X*-band EPR and the maximal dose variation was estimated to a factor of 3.5 between the distal and proximal parts of the phalanx.

II.D. EPR imaging

The EPR images were acquired at room temperature using an EPR Elexsys E540 System (Bruker, Rheinstatten, Germany) with three orthogonal water-cooled cylindrical gradient coils. The samples were positioned in the center of an *X*-band EPR superhigh *Q* cavity cylindrical resonator (ER 4122SHQE, 10 mm diameter) operating at ~9.5 GHz.

The maximum microwave power level (13 mW) was selected in the linear part of the power saturation curve previously measured. Power was optimized for each sample and ranged from 2.0 to 13.0 mW. Modulation amplitude was set to 0.25 mT for all samples, below one-third of the linewidth of the EPR signal for CO_2^- radicals (1.2 mT) to avoid signal broadening. Other parameters were as follows: 100 kHz modulation frequency, time constant ranged from 5.12 to 81.92 s, conversion time ranged from 5.12 to 10.24 s, 512 points, number of scans ranged from one to five, pixel size of 0.6 mm, and a 25 mm spatial window (field of view). Gradient strength was 340 mT m^{-1}. Nonirradiated bone samples were imaged using the same parameters. An acquisition was also performed using 0.7 mT of modulation and 25 scans instead of 3.

2D and 3D images were reconstructed from a complete set of projections collected as a function of the magnetic field gradient (340 mT m^{-1}) using a convoluted backprojection algorithm.[29] Spectral deconvolution and filtered backprojection were performed using the XEPR® software package (Bruker, Rheinstatten, Germany).

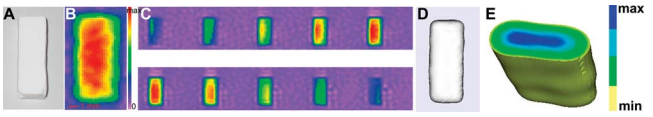

FIG. 1. (a) Original hydroxyapatite phantom. (b) 2D image of phantom homogeneously irradiated with x rays (100 Gy). (c) Contiguous slices from a 3D acquisition. Slice thickness is 0.5 mm. (d) 3D surface view. (e) Transverse cross section in the full volume phantom reconstructed from a 3D acquisition.

2D images were reconstructed on a 128×128 matrix by filtered backprojection using a Shepp-Logan filter.[30] Before reconstruction, each projection was deconvolved using fast Fourier transformation with the measured zero-gradient spectrum in order to improve image resolution. To reduce noise amplification and avoid possible division by zero at high frequencies, a low pass filter was used. The deconvolution parameters, including the maximum cut-off frequency and the width of the window in the Fourier space, were set up after viewing the shape of all projections. Spectral deconvolution and filtered backprojection were performed using the XEPR software package (Bruker).

II.E. Resolution: Edge spread function determination

The spatial resolution was evaluated in terms of the edge spread function (ESF). ESF was determined following a procedure modified from the classical method used in MRI (Ref. 31) and from the work of Halpern and co-workers.[32–34]

Briefly, a parallelepiped phantom made from synthetic HAP was homogeneously irradiated (300 Gy) with an external x-ray beam. The size of the phantom was 1.0×1.0×4.0 cm^3. A 2D image of the phantom was reconstructed. The signal along a line perpendicular to the edge of the phantom was extracted from the image and the derivative was calculated. A nine point smoothing algorithm was used to obtain the derivative curve which was then fitted by a Gaussian function:

$$f(x) = \frac{1}{\sigma\sqrt{2\pi}} e^{-(x-\mu)^2/2\sigma^2}. \quad (1)$$

From the computed σ values, the full width at half maximum (FWHM) of the Gaussian curve was calculated from the following equation: FWHM=2.$\sigma\sqrt{2 \ln 2}$. All calculations and fitting were carried out using PRISM 4 from GraphPad Software Inc. (La Jolla, CA).

III. RESULTS

After homogeneous external irradiation, 2D EPR imaging shows an overall homogeneous spin density distribution in a phantom of HAP [Fig. 1(b)]. Contiguous slices from a 3D acquisition [Fig. 1(c)] and a cross section through a full 3D reconstructed volume [Fig. 1(e)] confirm this distribution but also reveal a loss of signal toward the edges of the phantom. Figures 2(a)–2(c) show results for samples irradiated with

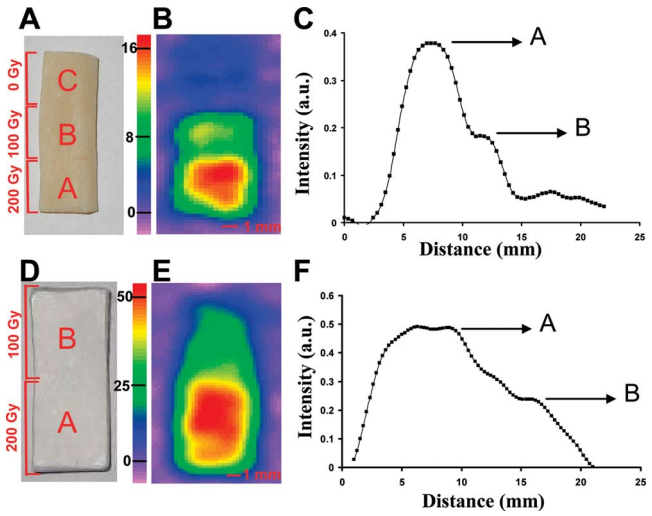

FIG. 2. (a) Bone sample irradiated at three different dose levels. (b) 2D EPR image. (c) Corresponding spin density profile extracted from 2D image along the long axis. (d) View of a hydoxyapatite phantom irradiated at 200 Gy (area *A*) and 100 Gy (area *B*). (e) 2D EPR image. (f) Corresponding spin density profile measured along the long axis of the sample.

stepwise gradients. Three zones of different signal intensities are clearly distinguishable [Fig. 2(b)] and correspond to the different areas irradiated at 200, 100, and 0 Gy [Fig. 2(a)]. The spin density curve could be extracted from the EPR image [Fig. 2(c)]. The ratio of signal intensity between areas *A* and *B* was 2.11, in close agreement with the actual delivered dose ratio.

The same observation was made for HAP phantoms. The signal ratio was 2.05 when the sample was irradiated at 200 and 100 Gy [Figs. 2(d) and 2(e)] and 1.93 when the delivered doses were 300 and 150 Gy. Signal smoothing was observed toward the edges of the samples and between the different irradiated areas, although we used sharp lead shielding to produce these stepwise gradients.

Figures 3 and 4 show the results for the continuous gradient experiments, induced with brachytherapy sources. When the source was centrally located, the distribution was symmetrical around the ^{125}I seed and the ^{192}Ir wire [Figs. 3(a)–3(d)]; it was asymmetrical (pear shaped) when the source was located on the side of the sample [Figs. 3(e)–3(h)]. Boundaries of the signal areas were highlighted by a dotted circle on the "iodine" images then copied onto the "iridium" images for ease of comparison. Signal distribution was slightly more widespread with bone samples than with HAP phantoms. A clear difference was observed between the images of ^{125}I and ^{192}Ir irradiated bone samples [e.g., Figs. 3(c) and 3(d)]. The difference was more visible when the source was located on the side because of the induced asymmetry of the irradiated zone [Figs. 3(e)–3(h)].

Some artifacts (concentric ring artifacts, star artifacts, etc.) are visible on some EPR images. The origin of these artifacts is multiple; they arise from limited angular sampling, from the cut-off frequency chosen for the Fourier transform used in the deconvolution process applied prior to image backprojection, etc. The intensity of these artifacts is mild and does not alter the qualitative information from these images.

Spin density profiles extracted from the EPR images (Fig. 4) reflect the shape of the dose gradient. In bones [Fig. 4(a)] and in HAP phantoms [Fig. 4(b)], ^{192}Ir sources located laterally gave a smooth curve with a longer range whereas ^{125}I (lateral position) showed steeper curves with a smaller range.

When distal phalanxes were externally irradiated with a continuous gradient, EPR imaging revealed an ambiguous spin density distribution (Fig. 5) with no apparent dose gradient. In contrast, several high intensity areas (spots) were distributed throughout the sample [Fig. 5(c)].

Resolution of the system was experimentally evaluated by the ESF. Figure 6 shows the signal intensity response along a line perpendicular to the edge of the parallelepiped phantom used for ESF measurement (black boxes) and its derivative (black curve). The first half of the curve was used for the Gaussian fitting. The σ value computed for the Gaussian fit of ESF was 0.796 ± 0.019; the goodness of fit (r^2) was 0.993. The corresponding calculated FWHM was 1.9 mm. The influence of the native EPR signal from the bone tissue was also investigated (Fig. 7).

Under the conditions used to acquire an image of an irradiated samples [Fig. 7(a)], a nonirradiated bone gives a very weak signal [more than a million time weaker, Fig. 7(b)]. The image represents mostly noise when normalized to its own maximum [Fig. 7(c)]. If the parameters of acquisition are changed, namely, by overmodulating the signal and by increasing the number of scans and the acquisition time, an image of rather good quality can be reconstructed even if its intensity remains lower by five orders of magnitude [Figs. 7(d) and 7(e)].

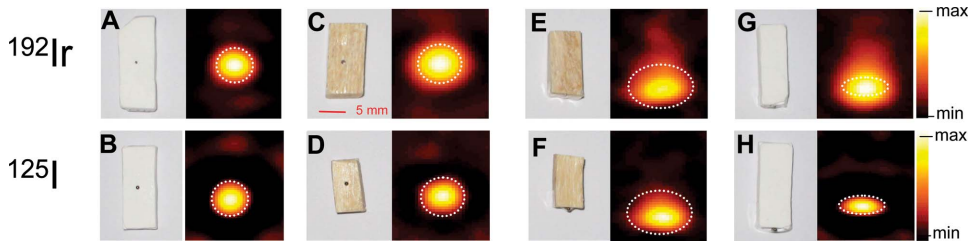

FIG. 3. 2D EPR images acquired from samples after gradient irradiation with iridium-192 (upper panels) and iodine-125 (lower panels). Sources were either located in the [(a) and (b)] center of HAP phantoms and [(c) and (d)] bone samples or on the side of [(e) and (f)] bones and [(g) and (h)] HAP phantoms. Images are normalized to their own maximum intensity.

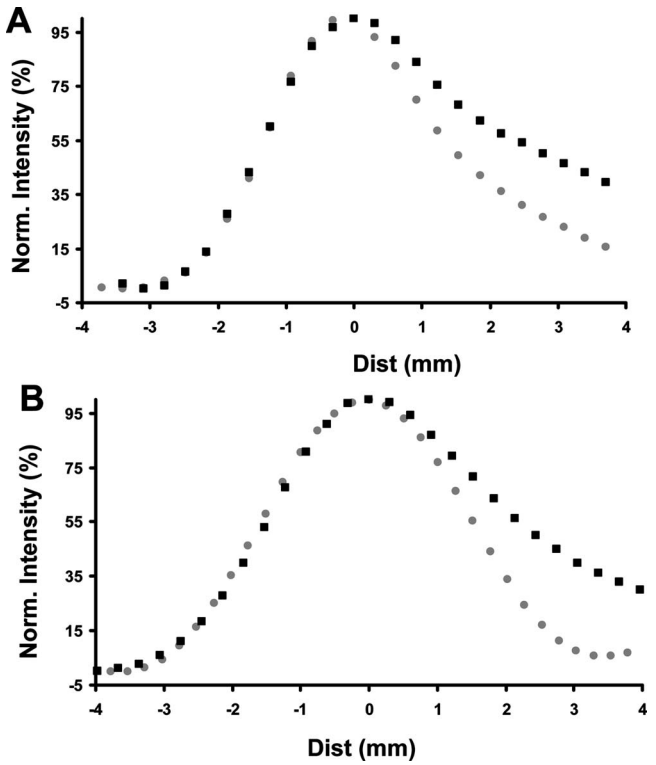

FIG. 4. Spin density curves extracted from 2D EPR images for (a) a typical bone sample or (b) HAP phantom. ^{192}iridium irradiation (black boxes) vs ^{125}iodine irradiation (gray circles).

IV. DISCUSSION

Homogeneous external irradiation using x rays should induce an even distribution of radicals in samples provided that the target sample structure is also homogeneous. We used samples of bone taken from the hardest part of the femur to ensure high tissue density and uniform density repartition in the sample. For control experiments, we needed a sample in which the HAP content would be controlled and also uniformly distributed. The use of phantoms made from compressed synthetic HAP was a practical way to satisfy this condition. Wave penetration in samples is usually a concern when working in the *X*-band EPR frequency domain. Here, in both types of sample, 2D EPRI gave images with a homogeneous distribution of the spin density throughout the sample volume as confirmed by 3D imaging. The EPR signal reflects the dose distribution unambiguously, at least if tissue density is constant and is not limited by wave penetration.

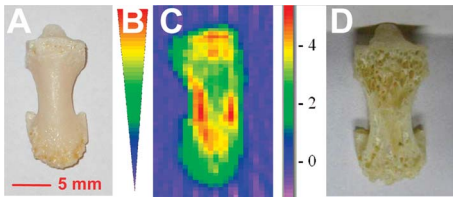

FIG. 5. (a) Terminal phalanx submitted to (b) external gradient irradiation and (c) its corresponding 2D EPR image. (d) Cross section across the bone sample reveals the spongy structure of the tissue.

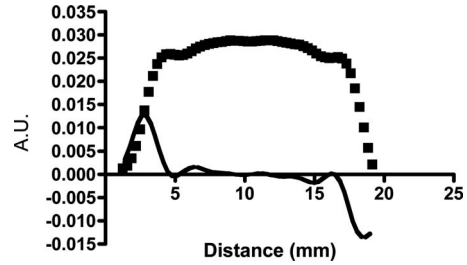

FIG. 6. EPR signal of a rectangular parallelepiped phantom made of hydroxyapatite, externally irradiated with x rays. The signal response (black boxes) is obtained along a line perpendicular to the edges of the phantom. Derivative curve after smoothing (black curve) was used for Gaussian fitting and calculation of the edge spread function.

Nevertheless, a marked fading of the signal toward the edges of the samples was observed. The same phenomenon occurred at the transition between areas submitted to different levels of irradiation, so that this transition zone is rather broad and does not show a clear-cut signal change (Fig. 2). These "edge effects" are most probably due to the limited resolution achieved with this kind of material. The linewidth of the EPR signal is around 1.1 mT which implies a theoretical resolution of 3 mm (FWHM) when using a field gradient of 340 mT m^{-1}. In our experiments, the expected resolution is better because deconvolution was used prior to back-projection and image reconstruction. The determination of the ESF gave an experimental resolution of 1.9 mm, better than the theoretical resolution. Slight spatial inhomogeneities of response of the EPR cavity that was used could also account for these variations in the signal toward the edges. There was proportionality of the EPR signal between areas irradiated under the stepwise dose gradient and signal ratios were consistent with the known delivered doses.

As deconvolution and reconstruction of images require the highest signal-to-noise ratio, we used *X*-band EPR in this first step of the validation process, because this modality offers a higher sensitivity over *L*-band EPR. The linewidth of the signal is independent of the modality used so that resolution is barely the same whatever the modality is used.

Brachytherapy sources were used to produce different gradient irradiation schemes. ^{125}I is a low energy emitter (35 keV) with relatively low penetrating radiations and is

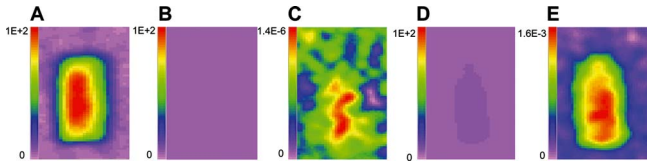

FIG. 7. Comparison of image intensities between irradiated and nonirradiated samples. (a) Image of an irradiated bone sample, normalized to its own maximum value. (b) Image of a nonirradiated bone sample, normalized to the maximum intensity of image (a). Same acquisition parameters as in (a). (c) Same image as (b) but normalized to its own maximum value. (d) Nonirradiated bone sample acquired with overmodulation (0.7 mT) and an accumulation of 25 scans. The intensity is normalized to the maximum value of image (a). (e) Same image as (d) but this time normalized to its own maximum value. Note the difference in scale intensity.

known to produce a steep gradient of dose deposition within tissue. In contrast, ^{192}Ir is a high energy gamma emitter (~350 keV) and produces a smoother gradient.

Spin density curves measured by EPRI matched the expected characteristics for both isotopes and a difference in ranges between these sources could be observed (Fig. 4). The curves are somewhat smoothed, as is clearly seen when the source was stuck to the side of the sample. Overall the methodology was sensitive enough to demonstrate a difference between gradient profiles within relatively short distances.

For irradiated phalanxes, there was an apparent absence of gradient on the EPR images (Fig. 5). This may be explained by a variation in the bone tissue density in this particular type of bone, inducing a variation in EPR signal distribution. The EPR signal comes from CO_2^- radicals induced by radiation in the mineral part of the bone, namely, HAP. Variation in bone density, and consequently in HAP content, will also result in a variation in the EPR signal, even with external homogeneous irradiation. The structure of the phalanx is spongy [Fig. 5(d)], with very high variation in tissue density. This can certainly be a confounding factor. A higher signal is seen at the edges and in other areas where bone density is higher. EPRI should be corrected for bone density variation in order to accurately depict dose distribution without the influence of tissue density variations. Coregistration and weighting with a CT scan image showing bone density distribution could greatly improve the method.

In conclusion, our study demonstrates that EPRI can be used to assess the regional relative dose distribution in irradiated bone samples. The signal-to-noise ratio that we obtained is fully acceptable in the dose range tested (100–300 Gy) and allows differentiation among sources that give different dose gradient profiles. The method is currently of limited accuracy for bones with high variation in tissue density but could likely be improved by using multimodality imaging and image coregistration.

These *X*-band results are also limited to *ex vivo* samples and should be confirmed in the near future by *L*-band experiments for possible *in vivo* application. A key issue will certainly be to achieve absolute dosimetry. The additive dose method could be used, at least to demonstrate the feasibility. This method consists of several postirradiations of a sample and subsequent EPR measurements. A plot of the ESR signal versus dose is obtained and the unknown dose is obtained by extrapolation of this dose curve to the zero added dose axis. This method is nevertheless obviously not applicable to *in vivo* measurements. Alternatively, an external calibration curve could be built from a phantom made with several tubes containing bone material irradiated at different known dose levels.

EPR has been used for many years in *in vivo* research animal experiments and is now being considered for clinical development,[35] specifically in the area of dosimetry using a patient's teeth as the dosimeter.[36,37]

Other challenges when considering transferring the method into the clinical arena to assess dose gradients in victims, include

- use of low frequency (*L* band) allowing higher wave penetration into tissues to assess doses in the range 20–100 Gy,
- estimate of the bone density to relate the EPR signal to calcium density, and
- increase in resolution of EPR images by data postprocessing.[38,39]

[a]Author to whom correspondence should be addressed. Electronic mail: bernard.gallez@uclouvain.be; Telephone: 32-2-7647391; Fax: 32-2-7647390.

[1]J. C. Nenot, "Radiation accidents: Historical review 1950-2000," Radioprotection **36**, 431–450 (2001).
[2]I. A. E. Agency, *Accidental Overexposure of Radiotherapy Patients in Bialystok* (IAEA, Vienna, 2004).
[3]S. Derreumaux, C. Etard, C. Huet, F. Trompier, I. Clairand, J. F. Bottollier-Depois, B. Aubert, and P. Gourmelon, "Lessons from recent accidents in radiation therapy in France," Radiat. Prot. Dosim. **131**, 130–135 (2008).
[4]I. Clairand, C. Huet, F. Trompier, and J. F. Bottollier-Depois, "Physical dosimetric reconstruction of a radiological accident due to gammagraphy equipment that occurred in Dakar and Abidjan in summer 2006," Radiat. Meas. **43**, 698–703 (2008).
[5]H. Scherthan *et al.*, "Radiation-induced late effects in two affected individuals of the Lilo radiation accident," Radiat. Res. **167**, 615–623 (2007).
[6]IAE Agency, *The Radiological Accident in Lilo, International Atomic Energy Agency*, edited by IAEA (IAEA, Vienna, 2000), p. 103.
[7]R. A. Kleinerman, A. A. Romanyukha, D. A. Schauer, and J. D. Tucker, "Retrospective assessment of radiation exposure using biological dosimetry: Chromosome painting, electron paramagnetic resonance and the glycophorin a mutation assay," Radiat. Res. **166**, 287–302 (2006).
[8]I. Aubineau-Laniece, L. de Carlan, I. Clairand, A. Lemosquet, S. Chiavassa, N. Pierrat, M. Bardies, and D. Franck, "Current developments at IRSN on computational tools dedicated to assessing doses for both internal and external exposure," Radiat. Prot. Dosim. **115**, 522–529 (2005).
[9]S. Chiavassa, A. Lemosquet, I. Aubineau-Laniece, L. de Carlan, I. Clairand, L. Ferrer, M. Bardies, D. Franck, and M. Zankl, "Dosimetric comparison of Monte Carlo codes (EGS4, MCNP, MCNPX) considering external and internal exposures of the Zubal phantom to electron and photon sources," Radiat. Prot. Dosim. **116**, 631–635 (2005).
[10]F. Takahashi and A. Endo, "Numerical system utilising a Monte Carlo calculation method for accurate dose assessment in radiation accidents," Radiat. Prot. Dosim. **126**, 595–599 (2007).
[11]A. Roux, E. Gaillard-Lecanu, J. F. Bottollier-Depois, Q. Chau, F. Trompier, and L. Lebedev, "Qualification of a numerical anthropomorphic model dedicated to radiological accidents," Radioprotection **36**, 57–75 (2001).
[12]I. A. E. Agency, *The Radiological Accident in Yanango* (IAEA, Vienna, 2000).
[13]J.-F. Bottollier-Depois, E. Gaillard-Lecanu, A. Roux, Q. Chau, F. Trompier, P. Voisin, and P. Gourmelon, "New approach for dose reconstruction: Application to one case of localized irradiation with radiological burns," Health Phys. **79**, 251–256 (2000).
[14]A. Leonard, J. Rueff, G. B. Gerber, and E. D. Leonard, "Usefulness and limits of biological dosimetry based on cytogenetic methods," Radiat. Prot. Dosim. **115**, 448–454 (2005).
[15]M. Desrosiers and D. A. Schauer, "Electron paramagnetic resonance (EPR) biodosimetry," Nucl. Instrum. Methods Phys. Res. B **184**, 219–228 (2001).
[16]D. A. Schauer, M. F. Desrosiers, P. Kuppusamy, and J. L. Zweier, "Radiation dosimetry of an accidental overexposure using EPR spectrometry and imaging of human bone," Appl. Radiat. Isot. **47**, 1345–1350 (1996).
[17]F. Trompier, J. Sadlo, J. Michalik, W. Stachowicz, A. Mazal, I. Clairand, J. Rostkowska, W. Bulski, A. Kulakowski, J. Sluszniak, S. Gozdz, and A. Wojcik, "EPR dosimetry for actual and suspected overexposures during radiotherapy treatments in Poland," Radiat. Meas. **42**, 1025–1028 (2007).
[18]J. M. Brady, N. O. Aarestad, and H. M. Swartz, "In vivo dosimetry by electron spin resonance spectroscopy," Health Phys. **15**, 43–47 (1968).
[19]H. M. Swartz, "Long-lived electron spin resonances in rats irradiated at room temperature," Radiat. Res. **24**, 579–586 (1965).

[20]D. A. Schauer, A. Iwasaki, A. A. Romanyukha, H. M. Swartz, and S. Onori, "Electron paramagnetic resonance (EPR) in medical dosimetry," Radiat. Meas. **41**, S117–S123 (2006).
[21]O. Baffa, A. Kinoshita, F. C. Abrego, A. B. dos Santos, B. Rossi, and C. Graeff, "ESR dosimetry," AIP Conf. Proc. **724**, 41–52 (2004).
[22]M. Zdravkova, N. Crokart, F. Trompier, N. Beghein, B. Gallez, and R. Debuyst, "Non-invasive determination of the irradiation dose in fingers using low-frequency EPR," Phys. Med. Biol. **49**, 2891–2898 (2004).
[23]M. Zdravkova, G. Vanhaelewyn, F. Callens, B. Gallez, and R. Debuyst, "Multi-frequency electron paramagnetic resonance study of irradiated human finger phalanxes," Spectrochim. Acta, Part A **61**, 3131–3138 (2005).
[24]D. J. Lurie, "Techniques and applications of EPR imaging," in *Electron Paramagnetic Resonance*, edited by B. C. Gilbert, M. J. Davies, and D. M. Murphy (Royal Society of Chemistry, Cambridge, 2002), Vol. 18, pp. 137–160.
[25]S. S. Eaton and G. R. Eaton, "EPR imaging," in *Electron Paramagnetic Resonance*, edited by B. C. Gilbert, M. J. Davies, and K. A. McLaughlan (Royal Society of Chemistry, Cambridge, 2000), Vol. 17, pp. 109–129.
[26]B. B. Williams and H. J. Halpern, "In vivo EPR imaging," *Biological Magnetic Resonance*, edited by S. R. Eaton, G. R. Eaton, L. J. Berliner (Kluwer Academic, New York, 2005), Vol. 23, pp. 283–319.
[27]E. S. Vanea, P. Leveque, F. Abboud, A. Bol, J. M. Denis, N. Kolbun, S. Vynckier, and B. Gallez, "Evaluation of the dose distribution gradient in the close vicinity of brachytherapy seeds using electron paramagnetic resonance imaging," Magn. Reson. Med. **61**, 1225–1231 (2009).
[28]E. Lund, H. Gustafsson, M. Danilczuk, M. D. Sastry, and A. Lund, "Compounds of ^{6}Li and natural Li for EPR dosimetry in photon/neutron mixed radiation fields," Spectrochim. Acta, Part A **60**, 1319–1326 (2004).
[29]P. T. Callaghan, *Principles of Nuclear Magnetic Resonance Microscopy* (Oxford University Press, Oxford, 1993).
[30]F. Natterer, *The Mathematics of Computerized Tomography* (Wiley, New York, 1986).
[31]D. W. McRobbie, E. A. Moore, M. J. Graves, and M. R. Prince, *MRI. From Picture to Proton* (Cambridge University Press, Cambridge, 2003).
[32]K.-H. Ahn and H. J. Halpern, "Simulation of 4D spectral-spatial EPR images," J. Magn. Reson. **187**, 1–9 (2007).
[33]K.-H. Ahn and H. J. Halpern, "Object dependent sweep width reduction with spectral-spatial EPR imaging," J. Magn. Reson. **186**, 105–111 (2007).
[34]K.-H. Ahn and H. J. Halpern, "Spatially uniform sampling in 4-D EPR spectral-spatial imaging," J. Magn. Reson. **185**, 152–158 (2007).
[35]H. M. Swartz, N. Khan, J. Buckey, R. Comi, L. Gould, O. Grinberg, A. Hartford, H. Hopf, H. Hou, E. Hug, A. Iwasaki, P. Lesniewski, I. Salikhov, and T. Walczak, "Clinical applications of EPR: Overview and perspectives," NMR Biomed. **17**, 335–351 (2004).
[36]H. M. Swartz *et al.*, "In vivo EPR for dosimetry," Radiat. Meas. **42**, 1075–1084 (2007).
[37]B. B. Williams, A. Sucheta, R. Dong, Y. Sakata, A. Iwasaki, G. Burke, O. Grinberg, P. Lesniewski, M. Kmiec, and H. M. Swartz, "Experimental procedures for sensitive and reproducible in situ EPR tooth dosimetry," Radiat. Meas. **42**, 1094–1098 (2007).
[38]R. Ahmad, B. Clymer, D. S. Vikram, Y. Deng, H. Hirata, J. L. Zweier, and P. Kuppusamy, "Enhanced resolution for EPR imaging by two-step deblurring," J. Magn. Reson. **184**, 246–257 (2007).
[39]H. Hirata, M. Wakana, and H. Susaki, "Feasibility study of superresolution continuous-wave electron paramagnetic resonance imaging," Appl. Phys. Lett. **88**, 254103-1–254103-3 (2006).